Clim Dyn
DOI 10.1007/s00382-013-1838-1

The seasonal predictability of the Asian summer monsoon in a two-tiered forecast system

Vasubandhu Misra · H. Li

Received: 28 December 2012 / Accepted: 8 June 2013

Abstract An extensive set of boreal summer seasonal hindcasts from a two tier system is compared with corresponding seasonal hindcasts from two other coupled ocean–atmosphere models for their seasonal prediction skill (for precipitation and surface temperature) of the Asian summer monsoon. The unique aspect of the two-tier system is that it is at relatively high resolution and the SST forcing is uniquely bias corrected from the multi-model averaged forecasted SST from the two coupled ocean–atmosphere models. Our analysis reveals: (a) The two-tier forecast system has seasonal prediction skill for precipitation that is comparable (over the Southeast Asian monsoon) or even higher (over the South Asian monsoon) than the coupled ocean–atmosphere. For seasonal anomalies of the surface temperature the results are more comparable across models, with all of them showing higher skill than that for precipitation. (b) Despite the improvement from the uncoupled AGCM all models in this study display a deterministic skill for seasonal precipitation anomalies over the Asian summer monsoon region to be weak. But there is useful probabilistic skill for tercile anomalies of precipitation and surface temperature that could be harvested from both the coupled and the uncoupled climate models. (c) Seasonal predictability of the South Asian summer monsoon (rainfall and temperature) does seem to stem from the remote ENSO forcing especially over the Indian monsoon region and the relatively weaker seasonal predictability in the Southeast Asian summer monsoon could be related to the comparatively weaker teleconnection with ENSO. The uncoupled AGCM with the bias corrected SST is able to leverage this teleconnection for improved seasonal prediction skill of the South Asian monsoon relative to the coupled models which display large systematic errors of the tropical SST's.

Keywords ENSO · Monsoon · Seasonal predictability

V. Misra (✉) · H. Li
Department of Earth, Ocean and Atmospheric Science, Florida State University, P.O. Box 3064520, Tallahassee, FL 32306-4520, USA
e-mail: vmisra@fsu.edu

V. Misra · H. Li
Center for Ocean-Atmospheric Prediction Studies, Florida State University, 2035 E. Paul Dirac Dr., 200 RM Johnson Bldg., Tallahassee, FL 32306-2840, USA

V. Misra
Florida Climate Institute, Florida State University, 2035 E. Paul Dirac Dr., 200 RM Johnson Bldg., Tallahassee, FL 32306-2840, USA

1 Introduction

The Asian summer monsoon is an important component of the global climate system, given its planetary scale influences (Krishnamurti and Ramanathan 1982; Webster 2006; Trenberth et al. 2006). Additionally the seasonality of the Asian summer monsoon and its relative abundance of rainfall have sustained a large human population for a very long time (Clift and Plumb 2008). Furthermore, it continues to be a region of the planet with the fastest growing human population. All of these factors make prediction of the Asian summer monsoon at all temporal scales extremely relevant. In this paper we discuss exclusively on the seasonal prediction skill of the Asian summer monsoon.

Ever since the early studies of Sperber and Palmer (1996) and Gadgil and Sajani (1998) on climate model intercomparison studies of the monsoon precipitation there have been several more related studies in the last decade

Published online: 20 June 2013

(Sperber et al. 2001; Kang et al. 2002; Waliser et al. 2002; Wang et al. 2004, 2009; Annamalai et al. 2007; Zhou et al. 2009; Kim et al. 2012). In several of these studies a common conclusion is that majority of the models have a tendency to rain more in the equatorial Indian Oceans than over the continental monsoon region. Furthermore it is repeatedly shown in these studies that the simulation of the monsoon winds is far more reasonable than that of the precipitation. So it is well known that monsoon simulation and therefore its prediction is a challenging issue confronting our field for some time (Webster et al. 1998; Wang et al. 2005).

There are several distinct ideas on the seasonal predictability of the monsoon. One is that the interannual variability of the monsoon is dictated by the external forcing of the El Niño and the Southern Oscillation (ENSO; Walker and Bliss 1932; Sikka 1980; Shukla and Paolino 1983; Meehl and Arblaster 2002; Annamalai and Liu 2005). However the stability of the monsoon-ENSO teleconnection has been of considerable interest (Krishnakumar et al. 1999; Krishnamurthy and Goswami 2000; Annamalai et al. 2007; Kucharski et al. 2007). Another school of thought is that the internal variability of the Asian monsoon is comparable to that of the externally forced component (Palmer 1994; Goswami 1998; Webster et al. 1998). Several studies also argue that local air-sea feedbacks are critical for successful simulation of the Asian monsoon (Wang et al. 2005; Kirtman and Shukla 2002; Wu and Kirtman 2005; Bracco et al. 2007; Misra 2008).

Sperber et al. (2001) indicate that the poor fidelity of the sub-seasonal variations of the Asian monsoon reflect in the poor skill of the dynamical seasonal prediction of the Asian monsoon. More recently Kim et al. (2012) find that the current operational climate models of National Centers for Environmental Prediction (NCEP) and European Center For Medium Range Weather Forecasting (ECMWF) suffer with a cold bias in the SST over the northern Indian and equatorial Pacific Oceans and a wet bias over the equatorial Indian Ocean and the Maritime region. They further indicate that ENSO modulation of the Asian monsoon in these climate models is stronger than observed. However several studies do indicate that the coupled ocean–atmosphere models are able to predict the large-scale features of the Asian monsoon variability reasonably (Wang et al. 2008a; Jiang et al. 2012). Wang et al. (2008a) identified two primary modes of the Asian monsoon variations viz., the first mode relating ENSO forcing of monsoon and the second mode relating the monsoon precursory conditions to ENSO. They find in comparing 10 contemporary coupled ocean–atmosphere models that both these modes are reasonably captured in terms of its seasonally evolving spatial patterns and interannual variations at 1-month lead time. However their variance is grossly underestimated.

In this paper we analyze the Asian monsoon seasonal predictability over its two subsystems from an extensive set of seasonal hindcasts conducted by three separate models. The two subsystems of the Asian monsoon, which is widely recognized, are the South Asian monsoon (that includes the Indian monsoon) and the Southeast Asian monsoon (Wang et al. 2003; Ding and Chan 2005). This distinction is made because the two subsystems vary in their land–ocean distribution, topography and interaction with mid-latitude climate variations, which make the regional monsoons of the two quite independent of each other (Tao and Chen 1987; Delworth and Manabe 1988; Wang et al. 2003; Ding and Chan 2005). Furthermore several studies have suggested a nuanced difference in the ENSO forcing of the two components of the Asian monsoon (Wang and Fan 1999; Wang et al. 2005; Jiang et al. 2012). These studies indicate that the ENSO forcing on the Southeast Asian monsoon is comparatively weaker than that over the South Asian monsoon.

The objective of this paper is to introduce a novel two tiered forecast system for monsoon prediction and compare its prediction skill with two single tiered (coupled ocean–atmosphere) models. The SST used to force the two-tiered Atmospheric General Circulation Model (AGCM) is actually borrowed from the forecasted SST of the two coupled ocean–atmosphere models with which it is compared. In the following section we describe the AGCM of the two-tiered system and a description of the seasonal hindcast experiments. Section 3 describes the results followed by concluding remarks in Sect. 4.

2 Description of model and seasonal hindcast experiments

The seasonal hindcasts initialized in late spring/early summer discussed in this paper stem from the Florida Climate Institute-Florida State University Seasonal Hindcasts at 50 km grid resolution (FISH50; Misra et al. 2013; Li and Misra 2013). FISH50 was conducted with the Florida Climate Institute-Florida State University Global Spectral Model (FGSM; Misra et al. 2013; Li and Misra 2013). The FGSM has 28 terrain following sigma levels, which is exactly similar in spacing to the NCEP-NCAR reanalysis model (Kalnay et al. 1996) and NCEP-DOE reanalysis model (Kanamitsu et al. 2002). They are unequal in vertical spacing, with higher resolution in the boundary layer and in the upper levels of the atmosphere, with the intervening layers being relatively coarser. The top of the atmosphere is located at around 1.3–2.5 hPa. The FISH50 was run at a spectral (triangular) truncation of T248 ($\sim$50 km grid resolution) with a time step of 5 min. A

Table 1 The physical parameterizations used in FGSM

Parameterization	Reference
Cumulus parameterization	Kain and Fritsch (1993), Kain (2004)
Shallow convection	Tiedtke 1983
Boundary layer	Hong and Pan 1996
Land surface	Ek et al. 2003
Gravity wave drag	Alpert et al. 1988
Shortwave radiation	Chou et al. 1996
Longwave radiation	Chou and Suarez 1994
Clouds	Slingo 1987

brief outline of the physics of the FGSM is provided in Table 1.

What makes FISH50 a unique two tiered seasonal hindcast dataset is that it has been computed in a "true" forecast mode unlike other two tiered seasonal predictability experiments, where either observed SST is used (Straus and Shukla 2002) or bias correction of SST is performed using observed climatology borrowed from the forecast period (LaRow 2013). Either way, the applicability of such a forecast system in an operational forecast environment is not practical as it borrows information from observations during the forecast season. In FISH50 we bias correct the multi-model averaged forecasted SST (from CCSM3 [Kirtman and Min 2009], CFSv2 [Saha et al. 2012]) using observations, but prior to the forecast season. The total SST used in FISH50 can be written as:

$$\mathrm{SST} = \mathrm{SST_{SC}} + \mathrm{SST_{LF}} + \mathrm{SST_{MMA}} \quad (1)$$

where, $\mathrm{SST_{SC}}$, $\mathrm{SST_{LF}}$, and $\mathrm{SST_{MMA}}$ are the stationary (climatological) observed seasonal cycle, observed low frequency variation (with periods >40 years), and multi-model averaged SST anomalies from the two coupled models respectively. The $\mathrm{SST_{SC}}$ component of observation is computed over the period 1880–1981. The $\mathrm{SST_{LF}}$ component of observation is computed over the period 1880 to the start of the seasonal hindcast, which is updated every year. Further details of this SST forcing dataset are provided in Misra et al. (2013) and Li and Misra (2013). Typically in other AGCM forced seasonal hindcasts $\mathrm{SST_{SC}}$ is computed over the forecast period (in our case 1981–2008) and is used in replacing the corresponding model predicted climatology (LaRow 2013).

In this paper we discuss only the summer seasonal hindcasts of FISH50. In FISH50 27 seasons were hindcasted between 1982 and 2008. Each season hindcasted in FISH50 had 6 ensemble members that differed only in the initial state of the atmosphere. Each of the ensemble members of FISH50 was initialized a day apart, starting from May 28 through June 3 of the year, using the NCEP-DOE reanalysis (Kanamitsu et al. 2002) for atmospheric initialization, which were interpolated to the FGSM grid. The land initial condition is identical in all 6 ensemble members of the FISH50 and are obtained from the NCEP-DOE reanalysis, which is again linearly interpolated to the FISH50 grid. The concentration of CO_2 was updated at the start of each seasonal hindcast following the observations from the Mauna Loa observatory (http://www.esrl.noaa.gov/gmd/ccgg/trends/index.html#global).

The results from FISH50 are compared with corresponding seasonal hindcasts from CCSM3 (Kirtman and Min 2009) and CFSv2 (Saha et al. 2012). The CCSM3 and CFSv2 seasonal hindcasts are run at T85 ($\sim$1.4°) and T126 ($\sim$1°) spectral truncation. At the time of conceiving FISH50, the seasonal hindcast of SST were available from only two of the current seven National Multi-Model Ensemble project (http://www.cpc.ncep.noaa.gov/products/ctb/MMEWhitePaperCPO_revised.pdf). In order to make fair comparisons between these three models we choose 6 ensemble members from both CFSv2 and CCSM3 from the available 24 and 10 ensemble members respectively. In case of CFSv2 we choose 6 ensemble members that match most closely with the start dates of FISH50 as the initial conditions for the ensemble members are staggered by 5 days in CFSv2 (Saha et al. 2012). But in the case of CCSM3 there is no preferred way to choose as all ensemble members have the same lead time for the forecast season following the methodology in Kirtman and Min (2009).

For verification of the seasonal hindcasts we use the monthly mean NCEP's Climate Prediction Center Merged Analysis of Precipitation (CMAP; Xie and Arkin 1997) available at 2.5° spatial resolution, which is available both over the oceans and land. However we choose to use the CMAP data for verification over the ocean only. Over land, we validate the models both for precipitation and surface temperature with the higher resolution University of Delaware (UD) monthly mean dataset (http://climate.geog.udel.edu/$\sim$climate/), which is available from 1901 to 2010 at 0.5° resolution. It should be noted that we interpolated all of these observations and the model hindcast data to the FISH50 grid.

3 Results

3.1 Surface temperature and precipitation climatology

In Fig. 1 we show the observed climatological seasonal mean June–July–August–September (JJAS) SST (Fig. 1a) and the corresponding SST bias from CFSv2 (Fig. 1b), CCSM3 (Fig. 1c) and FISH50 (Fig. 1d). The observations (Fig. 1a) show that the oceanic regions of the domain are characterized by very warm SST's (>27 °C) with

prevailing westerly zonal gradients over the tropical Indian Ocean. In CFSv2 (Fig. 1b) the far western Indian Ocean displays a very cold bias ($\sim$1.5 °C) that extends with relatively weaker cold bias into the central Indian Ocean and Bay of Bengal. On the other hand in western Pacific Ocean, CFSv2 displays a warm SST bias, resulting in an unobserved strong easterly SST gradient between the western Pacific and the Indian Oceans. In CCSM3 (Fig. 1c) the gradient of the SST bias is more complicated with warm bias displayed along coastal oceans of east Africa, cold bias in the Arabian Sea, Bay of Bengal, eastern Indian Ocean, south China Sea, and warm bias again over the Indonesian seas. By way of the bias correction in FISH50 (see Sect. 2) these SST biases have been largely removed and therefore in contrast to the two coupled models the SST bias is insignificant (Fig. 1d).

Figure 2a shows the observed climatological seasonal mean JJAS precipitation (CMAP over Oceans and UD over land), with three distinct regions of heavy rainfall areas including western coast of India, Bangladesh-northeastern India-Bay of Bengal-eastern equatorial Indian Ocean, the far southeastern Asian monsoon region and the surrounding oceanic regions. It is apparent from the figure that FISH50 (Fig. 2d) displays relatively higher bias than either of the two coupled models (Fig. 2b, c). The dry bias over the Gangetic plains over India is most widespread in FISH50 while the wet bias over the Southeast Asian monsoon is comparatively much higher (Fig. 2d). Even over the neighboring oceans the bias is significantly higher in FISH50.

Figure 3 shows the observed climatological seasonal mean JJAS near surface temperature and the corresponding bias in the three models. FISH50 again displays a relatively large warm bias over the Gangetic plains extending northwestward with weaker cold bias over the southern tip of India and Southeast Asia. CFSv2 also shows similar bias as FISH50 but with smaller magnitude, while CCSM3 indicates an overall cold bias over large parts of the South Asian monsoon region and parts of the Southeast Asian monsoon region.

3.2 Signal to noise ratio

The readers are referred to "Appendix" for the definition of the Signal to Noise (S/N) ratio used in this paper. The S/N ratio is a measure of the forced signal from external forcing (e.g. SST, soil moisture) relative to the ensemble spread for a given atmospheric variable. The ensemble spread in effect is a measure of the uncertainty of the hindcast. In this paper the uncertainty in the hindcast stems fundamentally from the uncertainty in the initial conditions only. So a small (large $\sim$1.0) S/N ratio would suggest that the ensemble spread is high (low) relative to the forced signal component in the variable. When the ensemble spread is large or the forced component is small we attribute it to higher contribution from the internal (or unforced component of the) variability.

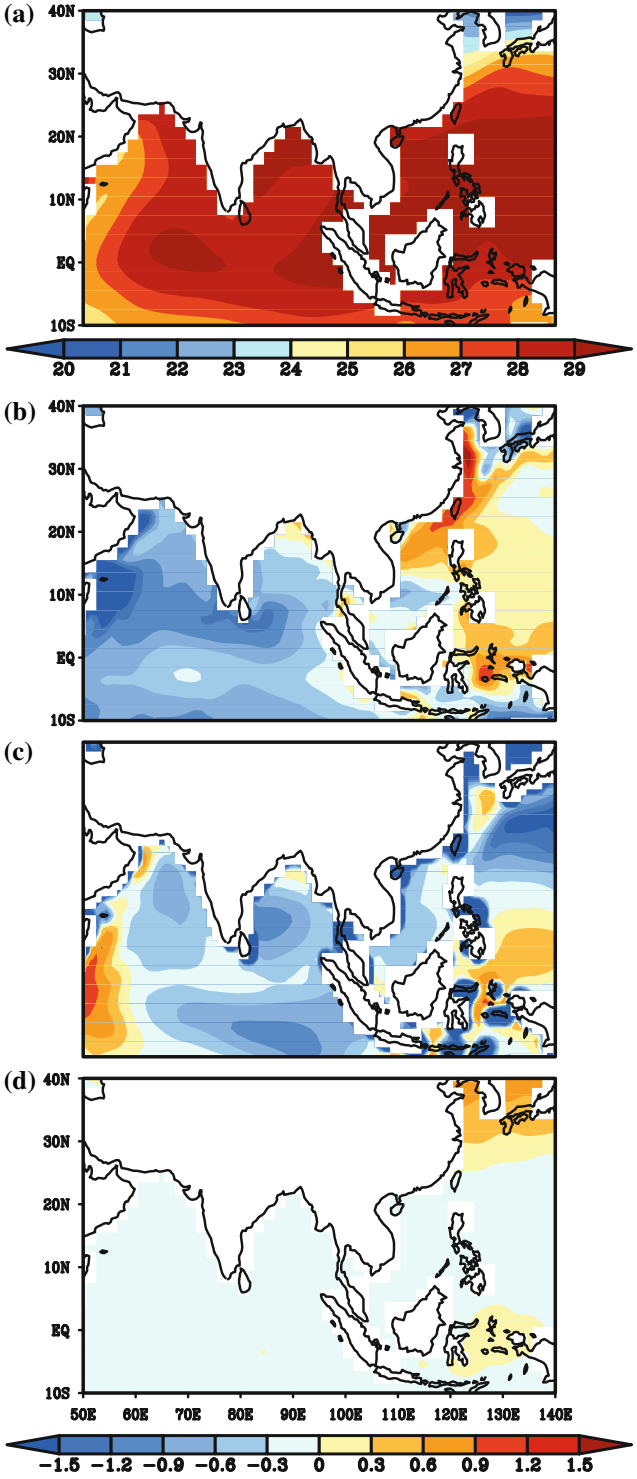

Fig. 1 The JJAS SST climatology (1982–2008) JJAS from (**a**) observation and the corresponding SST bias computed from (**b**) CFSv2, (**c**) CCSM3, and (**d**) FISH50. The units are in °C

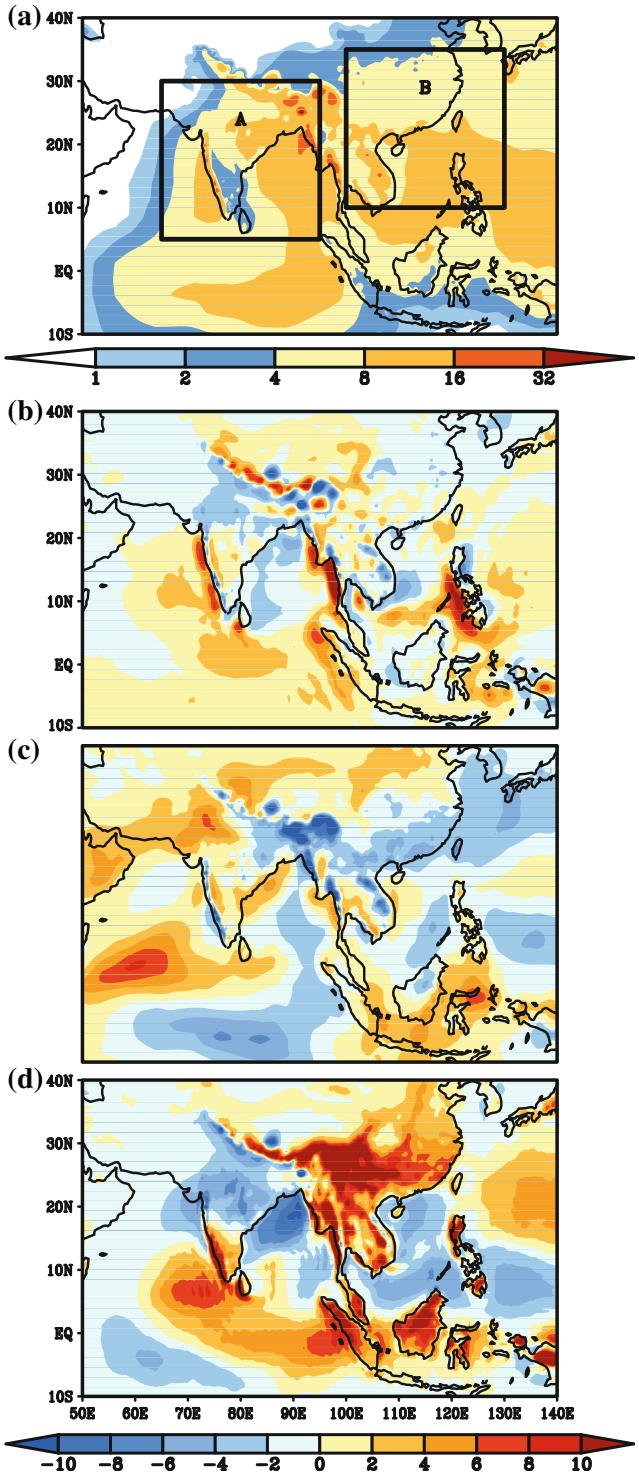

Fig. 2 **a** The observed JJAS climatology of precipitation (1982–2008) from University of Delaware over land and CMAP over ocean. The bias of the ensemble mean precipitation against observation for JJAS from seasonal hindcasts from **b** CFSv2, **c** CCSM3 and **d** FISH50. The units are in mm day^{-1}. The *box* over South Asian monsoon region (*box A*) and over far Southeastern Asian monsoon region (*box B*) in **a** are outlined for model diagnostics to be conducted specifically for those regions

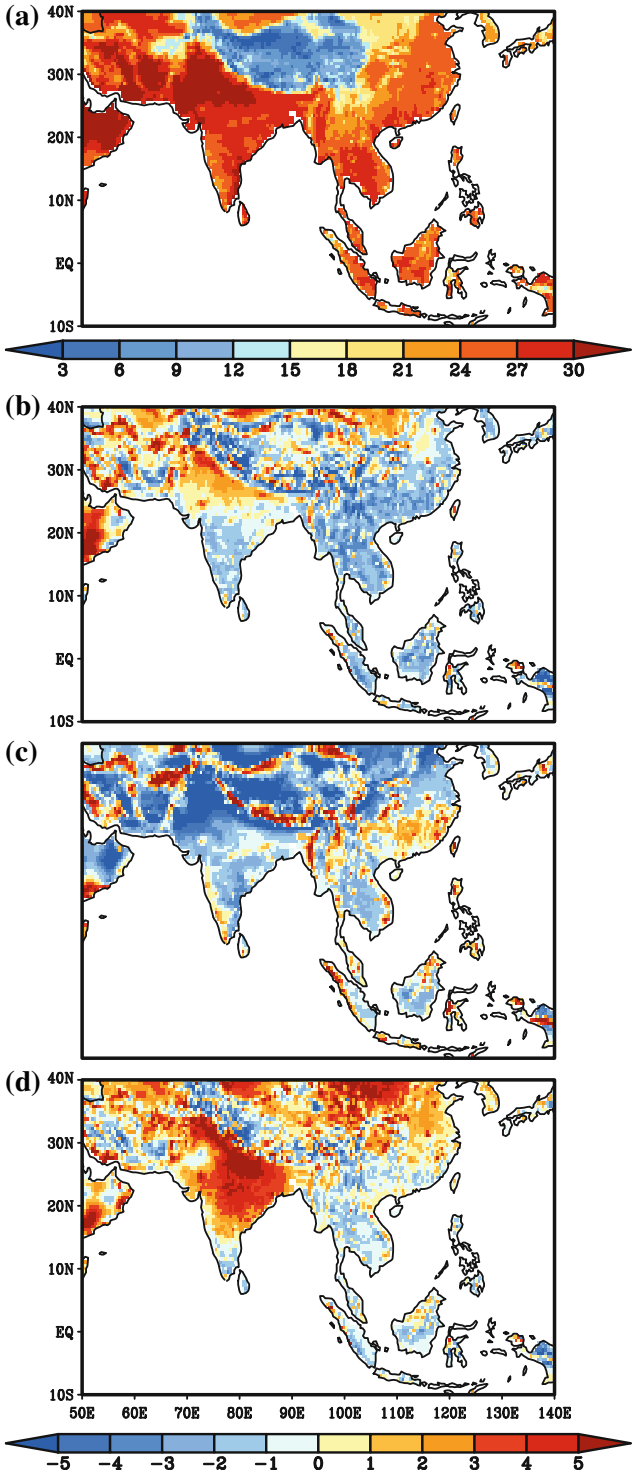

Fig. 3 **a** The JJAS T2 m climatology (1982–2008) from University of Delaware. The T2m bias climatology against observation from **b** CFSv2, **c** CCSM3 and **d** FISH50. The units are in °C

Figure 4 shows the spatial distribution of the S/N ratio of precipitation separately for land and ocean points of boxes A and B from the three models. It is worth men-

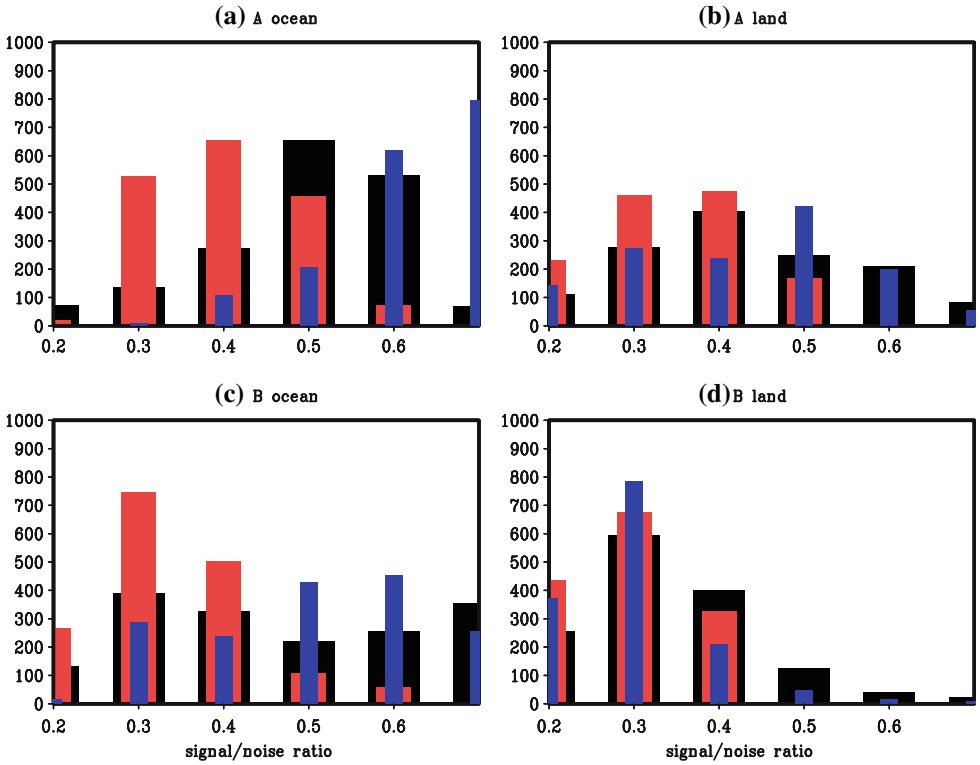

Fig. 4 The distribution of the signal to noise ratio for precipitation (shown as number of grid points on y-axis for a given range of the signal to noise ratio on X-axis) from FISH50, CFSv2, and CCSM3 for ocean and land points of *box A* and *B* (see Fig. 2a). FISH50 is in *black*, CFSv2 is in *red*, and CCSM3 is in *blue*. Precipitation from all models has been interpolated to the FISH50 grid for computing this figure

tioning again that the S/N ratio for this and subsequent figures were computed on the common grid of FISH50. Over oceans in box A (Fig. 4a) CCSM3 exhibits the largest fraction of the signal followed by FISH50. In comparison, over land in box A (Fig. 4b) the S/N ratio is proportionately less in all models, with a steep increase in the mid-range values (0.4–0.6) and a steep decline in the high range values (over 0.6). On the other hand the S/N ratio for ocean points in box B (Fig. 4c) display relatively lower S/N ratio compared to that in box A for all three models with CFSv2 displaying the least signal over oceans in box B. Similarly over land points in box B (Fig. 4d) the S/N ratio is relatively small compared to that over box A in all three models, with CFSv2 again showing the least signal in precipitation over land. In summary, JJAS mean precipitation over box A (for both ocean and land points) seems to be more strongly forced than over box B in all three models. Furthermore, the land points show less forced component of the seasonal mean precipitation than that over the oceans in both boxes in all three models.

Similarly, Fig. 5 shows the distribution of the S/N ratio for the mean JJAS surface temperature over land for the two boxes A and B. Again it is apparent from the figure that the land points in box A exhibit higher S/N ratio than that over box B. Furthermore, FISH50 and CFSv2 seem to display a higher forced signal in surface temperature than CCSM3 in both the boxes.

3.3 Deterministic skill analysis

Figure 6 shows the median[1] anomaly correlation of the seasonal mean JJAS precipitation for points with similar range of S/N ratio separately for land and ocean regions of boxes A and B. Ideally it would be desirable for the models to display a progressive increase in anomaly correlation with S/N ratio which would suggest that the model is justifiably confident in its most verifiable forecast. In Fig. 6a it is clearly seen that CFSv2 and FISH50 exhibit relatively high anomaly correlation that progressively increases with the increase in the S/N ratio over the ocean points in box A. In comparison, CCSM3 exhibits rather low anomaly correlation (Fig. 6a) despite the fact that it had comparatively a very large oceanic region with high S/N ratio (Fig. 4a). Over land (Fig. 6b) FISH50 exhibits progressively higher anomaly correlation at higher S/N ratio. CFSv2 also shows similar skill as FISH50 except that it has no land points in box A with S/N ratio greater than 0.6. But CCSM3 consistently exhibits a very weak (and even negative) anomaly correlation across the range of S/N ratio (Fig. 6b).

[1] The median value of anomaly correlation is a better choice than using average when correlations are aggregated from unequal number of points across models for a given range of S/N ratio (bins). Similarly, the median value is used in Figs. 7, 8, 11, 12.

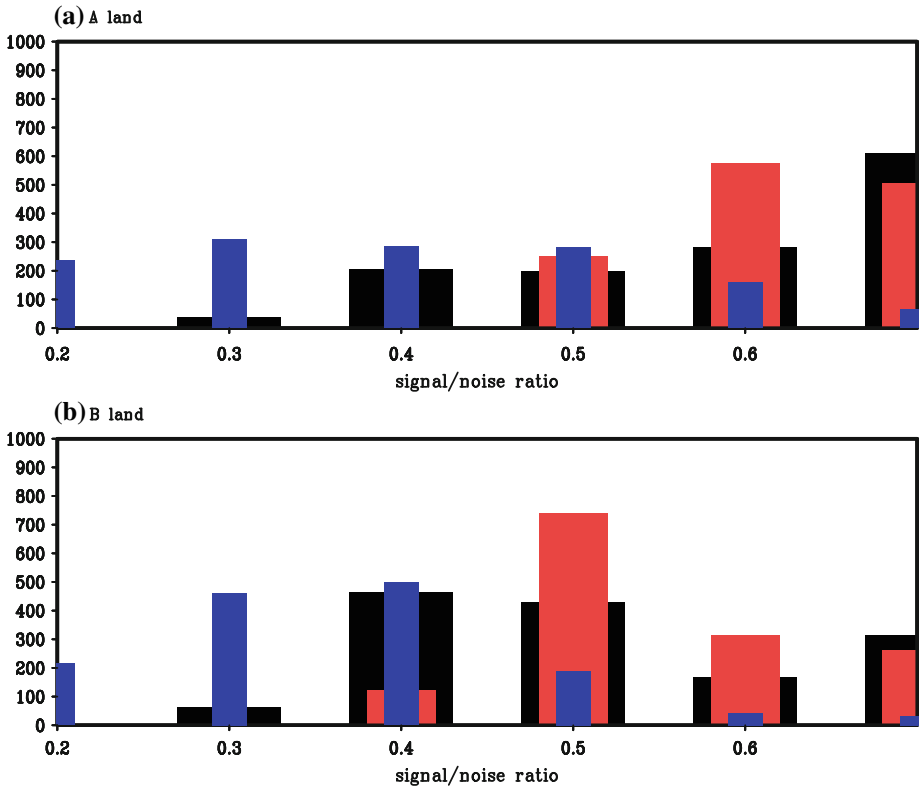

Fig. 5 Same as Fig. 4 but for near surface temperature over land points only

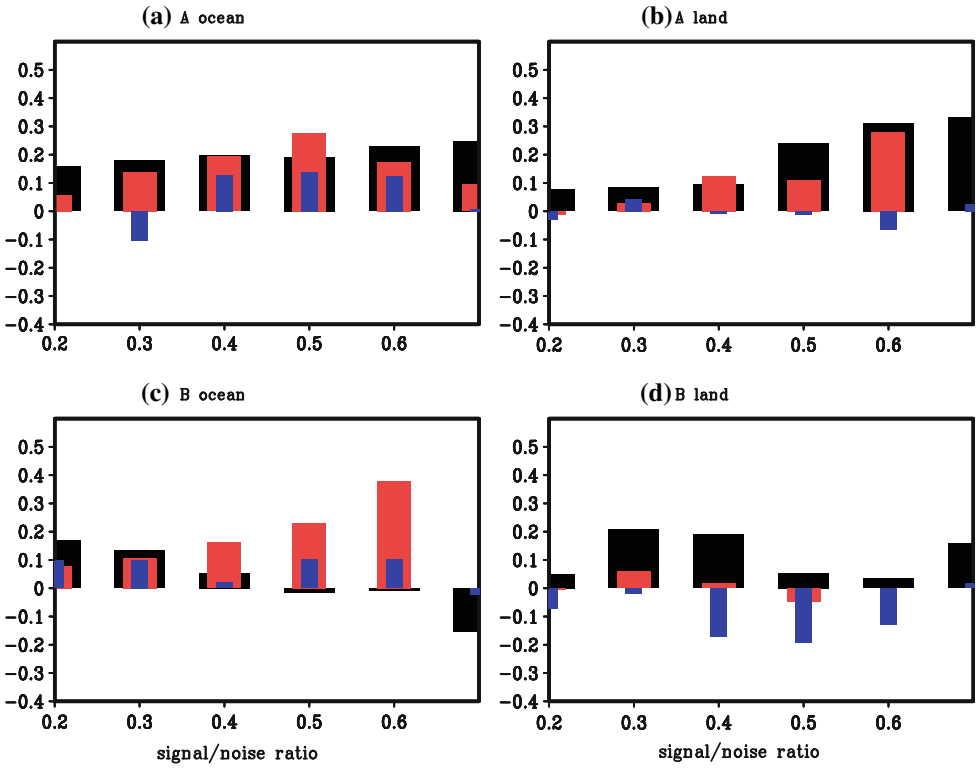

Fig. 6 The distribution of anomaly correlation (obtained as median value for a given range of signal to noise ratio) of the ensemble mean precipitation as a function of signal to noise ratios for FISH50, CFSv2, and CCSM3 for ocean and land points of *box A* and *B* (see Fig. 1). FISH50 is in *black*, CFSv2 is in *red*, and CCSM3 is in *blue*

Over the ocean points in box B (Fig. 6c), CFSv2 stands out in terms of its relatively high anomaly correlation and its progressive increase with increase in S/N ratio. FISH50 on the other hand displays a negative anomaly correlation at the highest S/N ratio range and has comparatively much weaker correlations than CFSv2 at lower S/N ratios. However over the land points in box B (Fig. 6d), the anomaly correlation displayed by CFSv2 and CCSM3 are

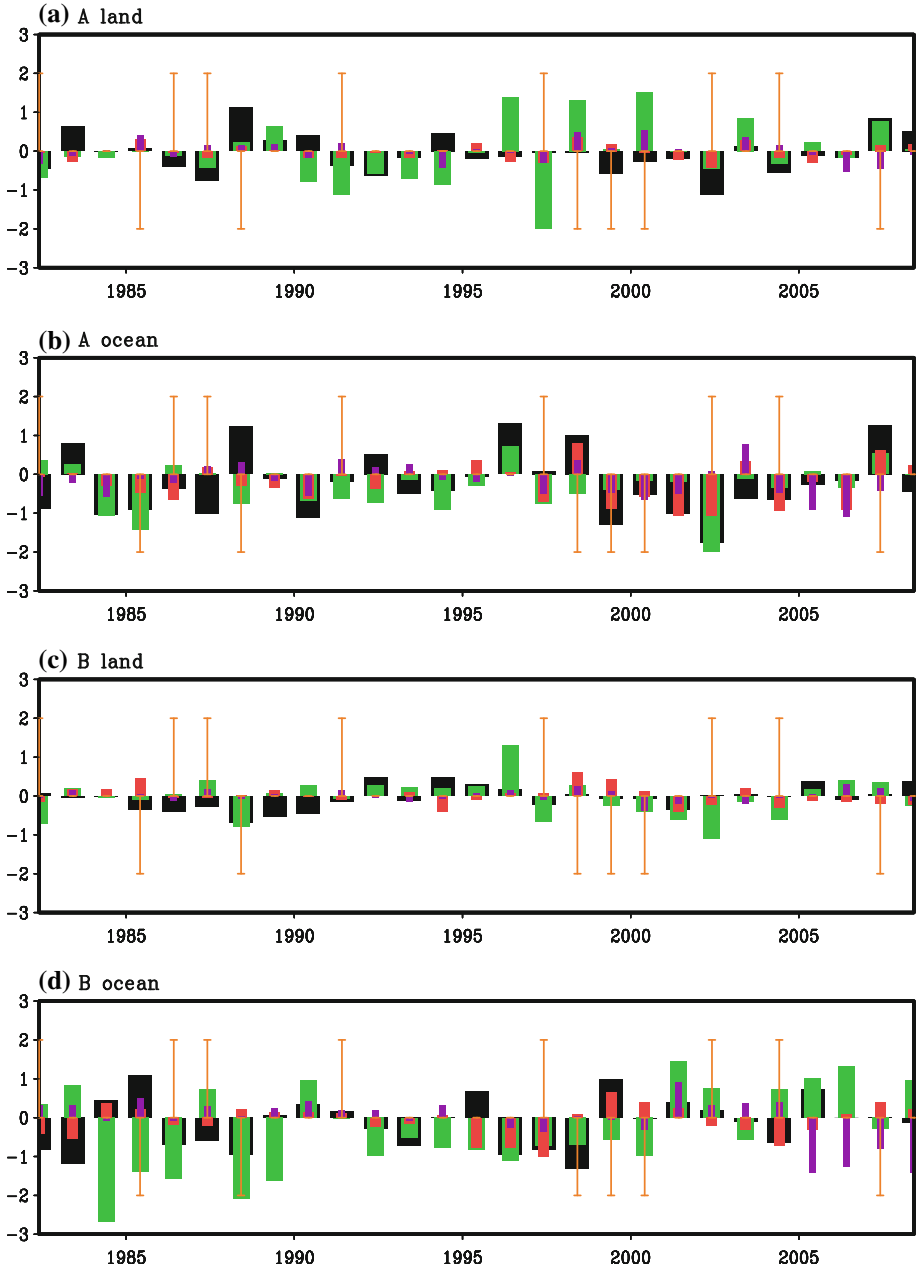

Fig. 7 The seasonal JJAS precipitation anomalies (obtained as the median value) for **a** land points in *box A*, **b** ocean points in *box A*, **c** land points in *box B*, and **d** land points in *box B* from the three models (FISH50: *green*; CFSv2: *red*; CCSM3: *purple*) and observations (*black*). The units are in mm day^{-1}. The ENSO years are shown in terms of the *orange bars*, with El Niño's (La Niña's) indicated by the *bars* above (below) the *zero line*

very weak (and even negative) across the range of S/N ratio while FISH50 displays positive correlations (albeit weak compared to the land points in box A) at all S/N ratios. We believe that this improvement in FISH50 relative to the other two models is an artifact of the use of higher spatial resolution model in FISH50, as the same type of verification using CMAP data showed FISH50 in a poor light relative to the other two models (not shown). In other words, FISH50 is able to resolve the spatial gradients of the seasonal precipitation anomalies over the Southeast Asian monsoon region. It may however be stated that in Fig. 4 all three models displayed a lower S/N ratio in box B than in box A. Alternatively, relative to box A, the models are less confident in their forecast of JJAS seasonal mean precipitation over box B. However the existence of negative or weaker correlation at higher S/N ratio undermines the deterministic forecast skill of the model, especially if there is significantly large number of grid points in the domain with high S/N ratio.

We also plotted the median value of the seasonal anomalies of precipitation for land and ocean points of the South (box A) and Southeast (box B) Asian monsoon domains (Fig. 7). The warm (cold) ENSO years (defined by seasonal JJAS Niño3 SST anomalies exceeding |0.5|) are indicated by the orange bars in the panels of Fig. 7. It is seen that in ENSO years the models typically follow the ENSO forcing on precipitation in the South Asian monsoon (box A) over both land and ocean (Fig. 7a, b) i.e., warm

(cold) ENSO years are associated with dry (wet) anomalies. The major exceptions to this teleconnection pattern (in Fig. 7a, b) are the JJAS seasons of 1997, 1998, 1999, and 2000. In the former two, the models followed the ENSO forcing and did not verify (both in sign and amplitude of the seasonal anomalies) with observations, while in the latter 2 years (1999 and 2000) the model predictions verified with the observations in sign over the oceans (Fig. 7b) but not over land (Fig. 7a). In comparison, the observed seasonal precipitation anomalies in the Southeast Asian monsoon region (box B; Fig. 7c, d) are smaller relative to that in box A both over the oceans and over land. They also don't have a strong ENSO forcing as in the case of box A, as a result of which the discrepancy (in the sign of the anomalies) between the observed and the predicted anomalies are apparent for more number of years than over box A.

It is obvious from the figure that FISH50 produces some of the largest seasonal anomalies across all domains. Both CFSv2 and CCSM3 display much smaller anomalies especially over land. In box A the skill shown by FISH50 at least over the land points (Fig. 6b) is leveraging from the ENSO forcing. And most of this skill (as measured by anomaly correlation) is seen more in predicting the sign of the anomalies, as the magnitude is invariably overestimated by FISH50.

Similarly the anomaly correlation of the JJAS seasonal mean surface temperature over land in box A and B from the three models are shown in Fig. 8. Here, unlike in the case of precipitation, all three models show a progressively increasing anomaly correlation with increasing S/N ratio, with CFSv2 displaying the highest anomaly correlation. The anomaly correlation of CCSM3 follows that of CFSv2 in box A (Fig. 8a) but not in box B (Fig. 8b). It is interesting to note that the number of grid points in the high range of S/N ratio in CCSM3 in comparatively low in both boxes A and B relative to the other two models. This implies that there are far fewer grid points in CCSM3 with high anomaly correlation of surface temperature in either of the two boxes than the other two models. In summary, from this analysis of deterministic skill of precipitation we observe that the two tier hindcast (FISH50) has some advantage over the two coupled models over land points of both the South Asian and the Southeast Asian monsoon regions. However, the deterministic skill of surface temperature in FISH50 although higher than that displayed for precipitation is marginally lower in skill than the CFSv2 in both boxes A and B, while CCSM3 displays rather poor skill over the Southeast Asian monsoon region.

3.4 Probabilistic skill analysis

Before the probabilistic skill analysis of the three models is presented we will discuss the practical significance of the tercile anomalies in precipitation and surface temperature. In precipitation (Fig. 9) and in surface temperature

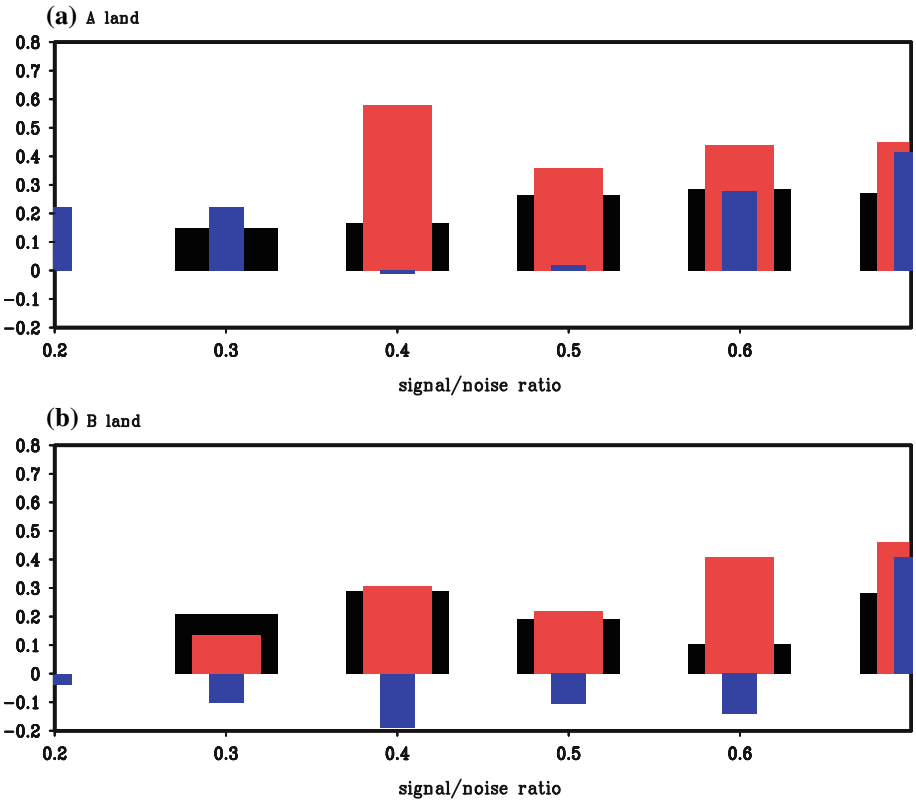

Fig. 8 Same as Fig. 6 but for near surface temperature over land

(Fig. 10) we notice that in both the observations and in the model forecasted JJAS seasonal mean tercile anomalies exceed one standard deviation over most part of boxes A and B. In both the coupled models however the tercile precipitation anomalies (Fig. 9c, d, g, h) are considerably lower than that in either the FISH50 (Fig. 9b, f) or the observations (Fig. 9a, e). FISH50 is able to capture the large extreme (both for high and low) tercile anomalies along the western coast of India and over Bangladesh as in the UD observations. However FISH50 seems to overestimate the extreme tercile values over the equatorial Oceans. In case of surface temperature, FISH50 (Fig. 10b, f) and CFSv2 (Fig. 10c, g) tercile anomalies are comparable to the observations (Fig. 10a, e) while in CCSM3

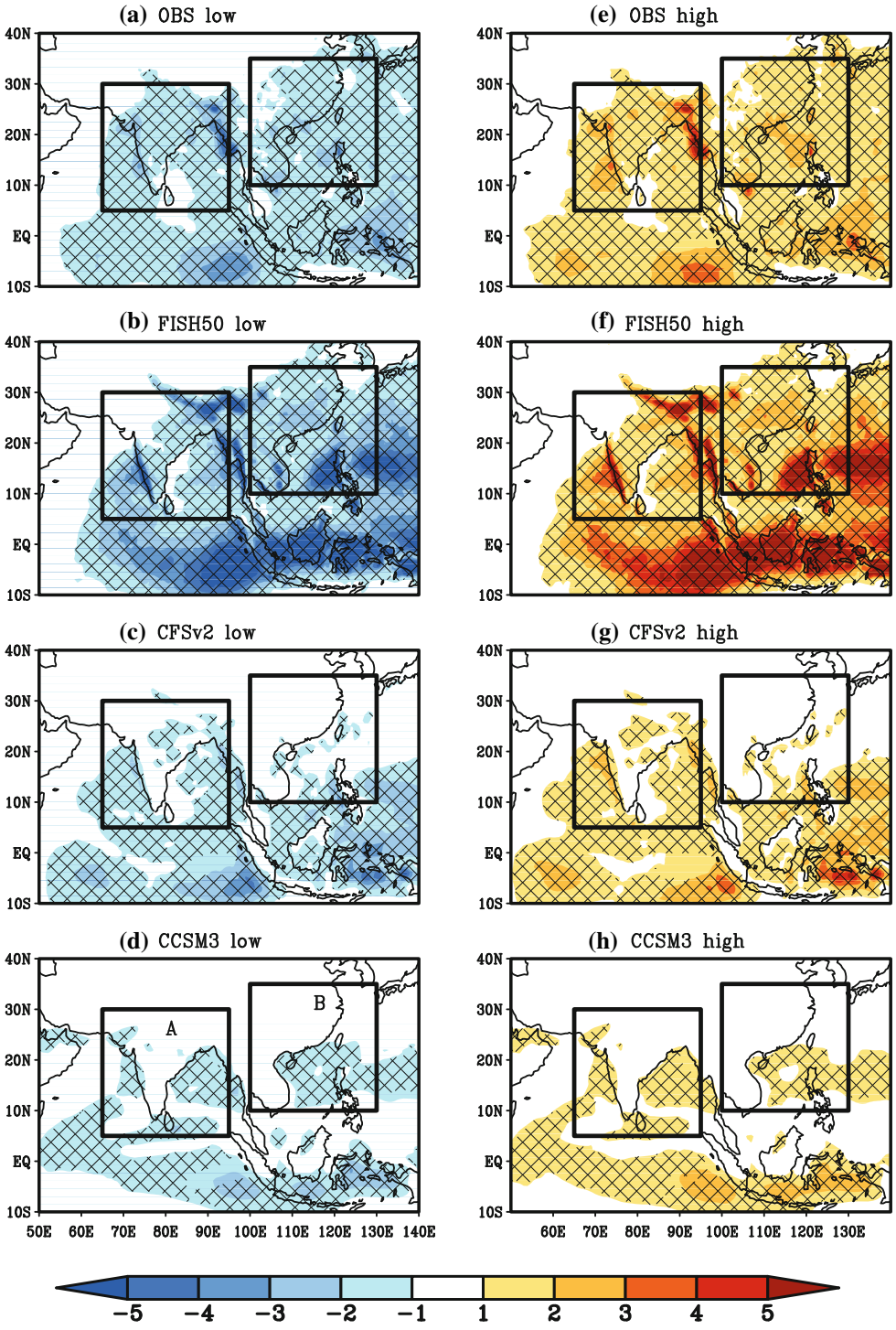

Fig. 9 The lower tercile precipitation anomalies (mm/day) for JJAS from **a** University of Delaware over land and CMAP over ocean, **b** FISH50, **c** CFSv2, and **d** CCSM3. Similarly the upper tercile precipitation anomalies (mm/day) for JJAS from **e** University of Delaware over land and CMAP over ocean, **f** FISH50, **g** CFSv2, and **h** CCSM3. The hashed region suggests that the rainfall anomaly for regions over 1 mm day^{-1} exceeds one standard deviation. The *boxes A* and *B* are *outlined*

(Fig. 10d, h) the anomalies continue to be underestimated. Nonetheless, the observations and FISH50 suggest that the tercile anomalies of these surface variables in the Indian and in the Southeast Asian monsoon region are meaningful in that they describe significant deviations (near or above one standard deviation) from the mean. Therefore in the rest of this subsection we will discuss the ability of the models to probabilistically forecast these tercile anomalies based on the Area under the Relative Operating Characteristic Curves (AROC; Mason and Graham 1999, 2002).

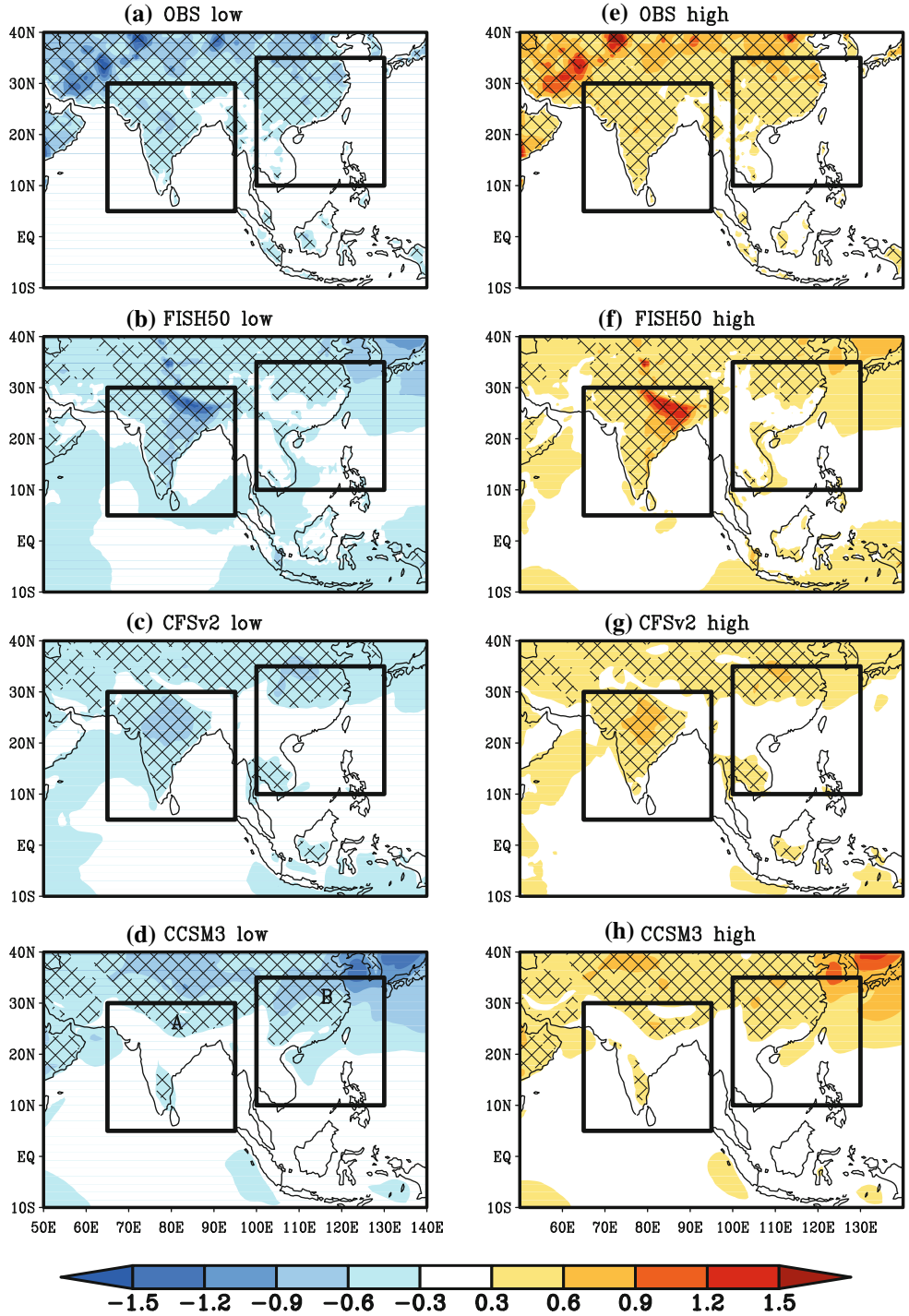

Fig. 10 Same as Fig. 8 but for surface temperature. The observations are from University of Delaware. The hashed regions indicate that the tercile anomalies over 0.3 °C exceed one standard deviation

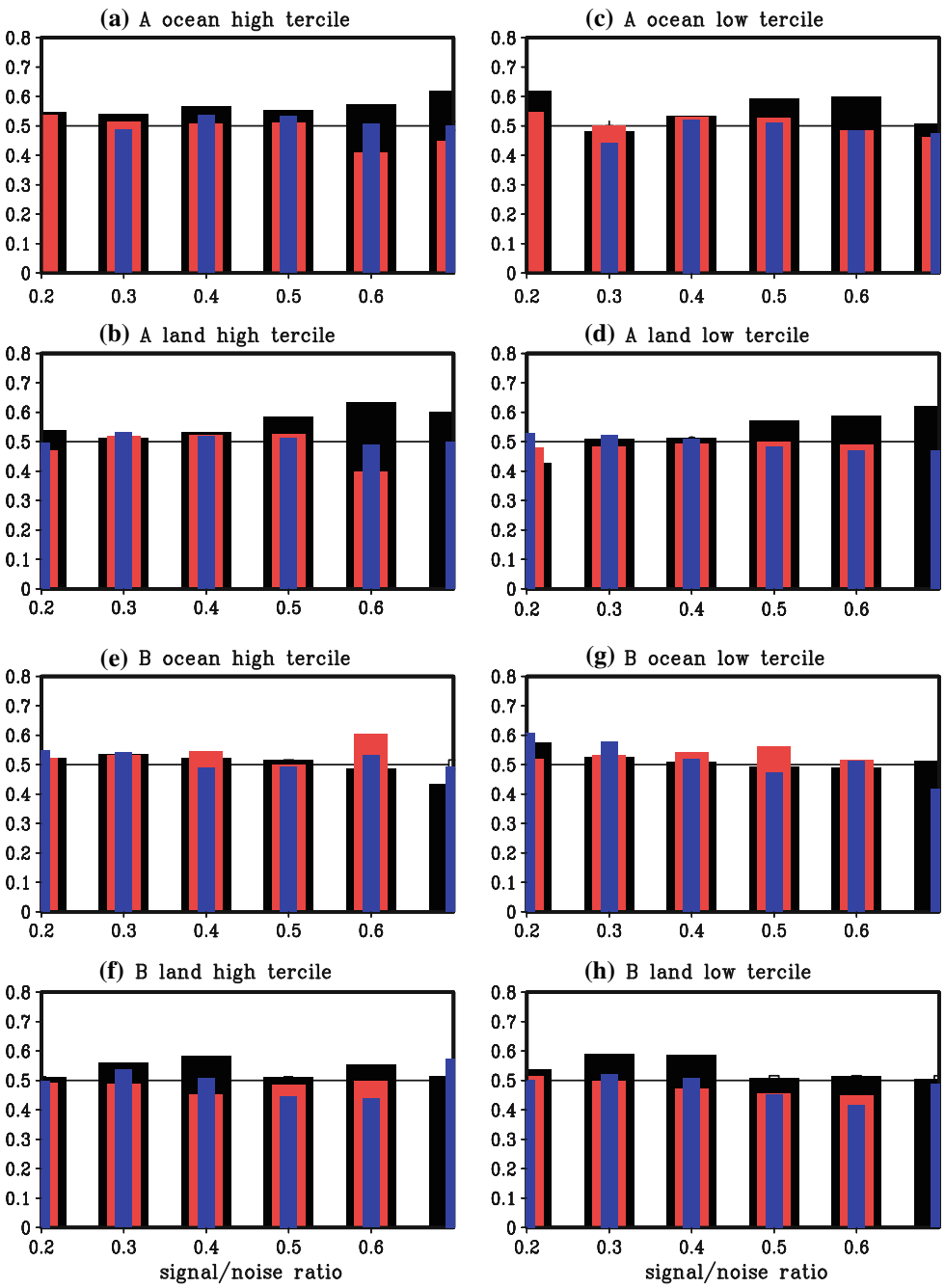

Fig. 11 The distribution of the median of the area under the relative operating characteristic curve for high (low) tercile JJAS mean precipitation anomaly events as a function of the signal to noise ratio for FISH50, CFSv2, and CCSM3 for ocean and land points of *box A* and *B* (see Fig. 2). FISH50 is in *black*, CFSv2 is in *red*, and CCSM3 is in *blue*. The *solid line* across the AROC value of 0.5 suggests the threshold for skills that distinguish it from climatology

Figure 11 show the distribution of the AROC for the high tercile seasonal mean JJAS precipitation anomaly as a function of the S/N ratio. Here unlike the anomaly correlation in Fig. 6, the distribution of AROC as a function of S/N ratio is largely flat over all domains and interestingly the skills are relatively more comparable across models. But FISH50 does exhibit a slight advantage over the other two models especially at higher S/N ratio over both land and ocean in box A for the extreme tercile anomalies (Fig. 11a–d). It is revealing that in this probabilistic skill analysis, the models display a marginal (but important) improvement over the climatological skill of AROC = 0.5 over box A for the extreme tercile anomalies especially at higher S/N ratios. Similarly, over box B, the models are showing a marginal increase over the climatological AROC skill (Fig. 11e–h).

Similarly the distribution of AROC for high and low tercile anomalies of surface temperature over land show a small but subtle improvement over the climatological skill at nearly all S/N ratios over boxes A and B (Fig. 12). Again

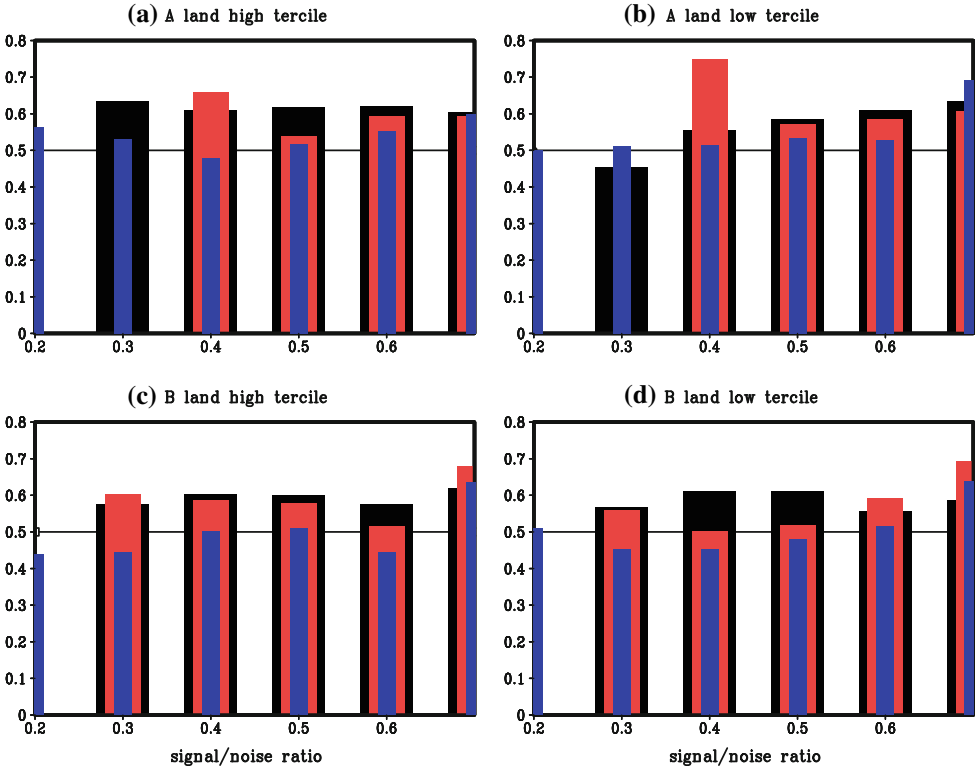

Fig. 12 Same as Fig. 11 but for near surface temperature over land

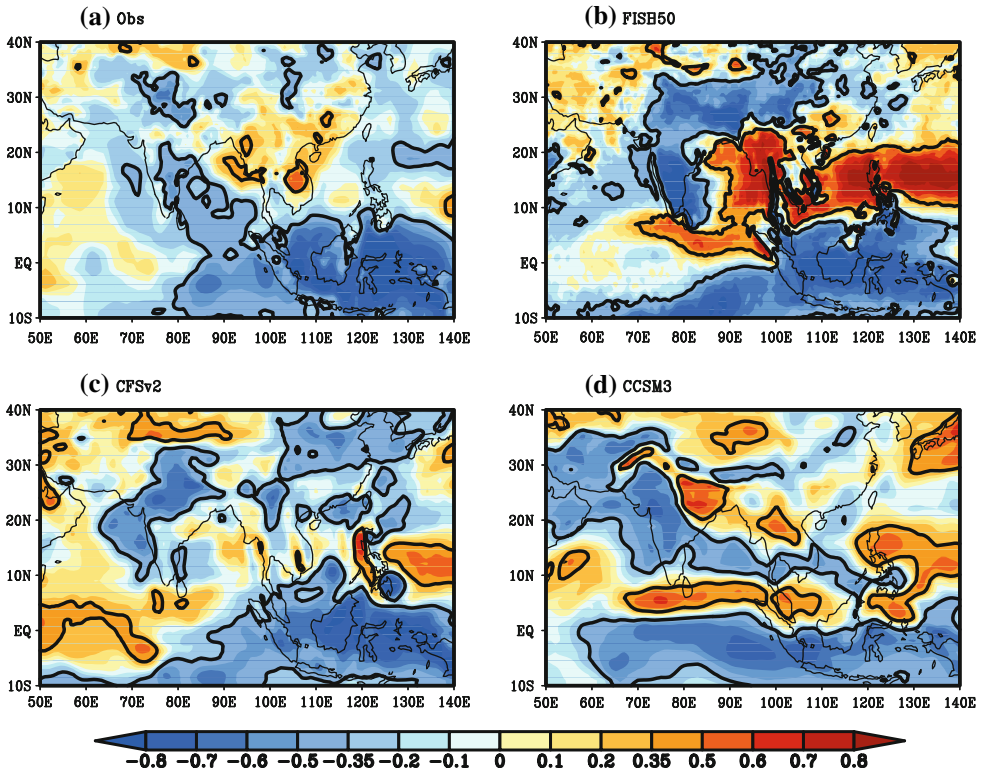

Fig. 13 The contemporaneous correlation between mean JJAS Niño3.4 index and precipitation from **a** observations, **b** FISH50, **c** CFSv2, and **d** CCSM3. Significant value over 10 % significance level according to student *t* test is contoured

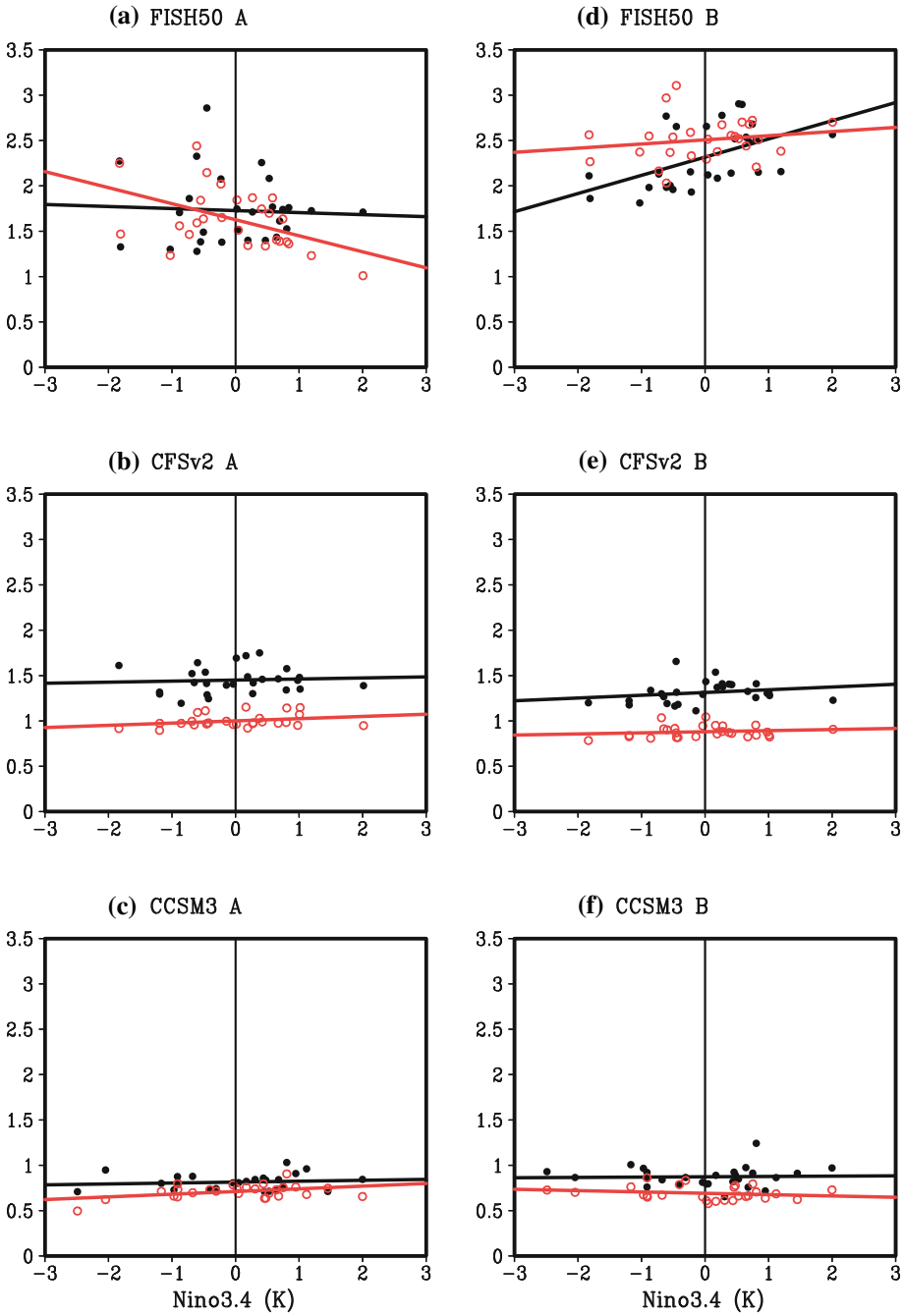

Fig. 14 The ensemble spread of precipitation (measured as the standard deviation about the ensemble mean for each season) as a function of the corresponding mean JJAS Niño3.4 SST index from the three models for ocean and land points in *boxes A* and *B* (see Fig. 2). Ocean is in *black*, and land is in *red*. The units of precipitation are in mm day^{-1} and that for SST anomalies is in Kelvins (K)

it is apparent that the probabilistic skill of all three models is nearly comparable, despite the varied systematic errors shown earlier.

In summary these probabilistic skill analysis suggests that some useful seasonal prediction skill of precipitation at least from FISH50 can be harvested despite a poor exhibition of deterministic skill over the Indian monsoon domain relative to climatology or persistence. In case of surface temperature, the results are more encouraging with AROC values consistently well above 0.5 in both boxes A and B for FISH50 and CFSv2.

4 Discussion and conclusions

FISH50 despite being a two-tier forecast system clearly demonstrates that it is comparable to the two coupled models in terms of its seasonal prediction skill of the seasonal mean precipitation anomalies and surface temperature anomalies over the Asian Monsoon region. In fact over the South Asian monsoon region, FISH50 demonstrates some advantage over the other two coupled models in terms of its precipitation anomalies especially over the land regions of the South and the Southeast Asian

monsoons. In order to investigate this further we computed the contemporaneous correlation of precipitation with the Niño3.4 index from the ensemble mean (Fig. 13). It is seen that all three models exhibit a relatively strong negative correlation over the Indian monsoon region while in the Southeast Asian monsoon region the correlations are comparatively weak, except in the case of FISH50, which shows an unobserved strong positive correlation over the South China and the Philippines Sea.

An obvious question is that in the presence of such teleconnection, what is its influence on the ensemble spread of the seasonal hindcast from the models? This is answered in Fig. 14, which shows the ensemble spread for precipitation from both boxes A and B as a function of the Niño3.4 SST index from the model hindcasts. For precipitation, the ensemble spread over land points in box A in FISH50 seems to indicate that warm Niño3.4 SST anomalies result in slightly less spread than the cold anomalies, while in the other two models the ensemble spread does not seem to show any relation with the Niño3.4 SST anomalies. Over the ocean, only FISH50 in box B seems to suggest that warm Niño3.4 SST anomalies seem to cause more spread than the cold anomalies (Fig. 14d). But we contend that this feature of FISH50 over box B is erroneous given the rather poor hindcast skill of FISH50 in box B and the erroneous positive correlation of precipitation over Southeast Asian monsoon domain with the Niño3.4 SST index (Fig. 13b). In some recent studies it is again being reinforced that the South Asian monsoon seasonal predictability skill is linked to the contemporaneous teleconnections with eastern equatorial Pacific SST anomalies (Delsole and Shukla 2012; Jiang et al. 2012; Kim et al. 2012).

In conclusion, we find that the remote ENSO forcing continues to offer the seasonal predictability of the Indian monsoon and the lack of such forcing in the Southeast Asian monsoon makes the latter's seasonal prediction a more difficult problem, reconfirming some of the earlier studies. We contend based on this study that the large systematic errors of tropical SST in the coupled models are likely the cause of them not being able to retain the remote ENSO forcing on the Indian summer monsoon to the same extent as in FISH50. Although admittedly FISH50 seems to show too strong a ENSO teleconnection with the South Asian monsoon than what is observed. The coupled air-sea interaction is germane to the Asian monsoon variability. However, the fidelity of our current coupled models are most likely not at a level where the local air-sea feedbacks could be shown clearly as an important component of the forecast system that improves the seasonal predictability of either the South or the Southeast Asian monsoon relative to two tier forecast system like FISH50. This study suggests that a two-tiered climate forecast system could be used as a benchmark to highlight the issues with the current coupled models and not necessarily promote them as an alternative tool for the monsoon prediction problem.

Acknowledgments This work was supported by grants from NOAA (NA12OAR4310078, NA10OAR4310215, NA11OAR4310110), USGS (06HQGR0125), and USDA (027865). All model integrations for this paper were done on the computational resources provided by the Extreme Science and Engineering Discovery Environment (XSEDE) under TG-ATM120017 and TG-ATM120010. The University of Delaware precipitation data was provided by the NOAA/OAR/ESRL PSD, Boulder, Colorado, USA, from their Web site at http://www.esrl.noaa.gov/psd/.

Appendix: Signal to noise ratio

The signal to noise ratio is an objective measure of an AGCM's predictability (Straus and Shukla 2000). It is basically a measure of the variance displayed by the ensemble mean relative to the ensemble spread of the seasonal hindcast. So higher values of this ratio correspond to higher predictability of the phenomenon by the AGCM. This measure of predictability however does not reflect on the verification of the hindcast or forecast. The ensemble mean for a given climate variable (say Y), for a given climate model, and for a given year j is:

$$\overline{Y_j} = \frac{1}{K}\sum_{i=1}^{K} Y_{\overline{N}}$$

where i is the index for number of ensemble members and K is the total number of ensemble members (in our study it is 6).

The variance of the ensemble spread for a given year j is given by:

$$\sigma_j^2 = \frac{1}{K}\sum_{i=1}^{K} (Y_{\overline{N}} - \overline{Y_j})^2$$

The variance of the ensemble spread is a measure of the noise in the forecast system, which is averaged over all years of the hindcast to obtain:

$$\sigma_{noise}^2 = \frac{1}{L}\sum_{j=1}^{L} \sigma_j^2$$

The variance of the signal component is given by:

$$\sigma_{signal}^2 = \frac{1}{L}\sum_{j=1}^{L} (\overline{Y_j} - \overline{Y})^2$$

where

$$\overline{Y} = \frac{1}{LK}\sum_{j=1}^{L}\sum_{i=1}^{K} Y_{\overline{N}}$$

Then, predictability (Π) or signal to noise ratio is defined as:

$$\prod = \frac{\sigma^2_{signal}}{\sigma^2_{signal} + \sigma^2_{noise}}$$

References

Saha S et al (2013) The NCEP climate forecast system Version 2. J. Climate. Submitted. Available from http://cfs.ncep.noaa.gov/cfsv2.info/CFSv2_paper.pdf

Alpert JC, Kanamitsu M, Caplan PM, Sela JG, White GH, Kalnay E (1988) Mountain induced gravity wave drag parameterization in the NMC medium-range model. Preprints, eighth conference on numerical weather prediction, Baltimore, MD. Am Meteor Soc: 726–733

Annamalai H, Liu P (2005) Response of the Asian Summer Monsoon to changes in El Niño properties. Quart J R Meteor Soc 131:805–831

Annamalai H, Hamilton K, Sperber KR (2007) The South Asian summer monsoon and its relationship with ENSO in the IPCC AR4 simulations. J Clim 20:1071–1092

Bracco A, Kucharski F, Molteni F, Hazeleger W, Severijns C (2007) A recipe for simulating the interannual variability of the Asian Summer Monsoon and its relation with ENSO. Clim Dyn 28:441–460. doi:10.1007/s00382-006-0190-0

Chou M-D, Suarez MJ (1994) An efficient thermal infrared radiation parameterization for use in general circulation models. Technical report series on global modeling and data assimilation, NASA/TM-1994-104606, vol 3, p 85

Chou M-D, Lee K-T, Tsay S-C, Fu Q (1996) Parameterization for cloud long wave scattering for use in atmospheric models. J Clim 12:159–169

Clift PD, Plumb AJ (2008) The Asian monsoon: causes, history and effects. Cambridge University Press, Cambridge

DelSole T, Shukla J (2012) Climate models produce skillful predictions of Indian summer monsoon rainfall. Geophys Res Lett 39:L09703. doi:10.1029/2012GL051279

Delworth TL, Manabe S (1988) The influence of potential evaporation on the variabilities of simulated soil wetness and climate. J Clim 1:523–547

Ding Y, Chan JCL (2005) The East Asian summer monsoon: an overview. Meteor Atm Phys 89:117–142

Ek MB, Mitchell KE, Lin Y, Rogers E, Grunmann P, Koren V, Gayno G, Tarpley JD (2003) Implementation of Noah land surface model advances in the National Centers for Environmental Prediction operational mesoscale Eta model. J Geophys Res 108:8851. doi:10.1029/2002JD003296

Gadgil S, Sajani S (1998) Monsoon precipitation in the AMIP runs. Clim Dyn 14:659–689

Goswami BN (1998) Interannual variations of Indian summer monsoon in a GCM: external conditions versus internal feedbacks. J Clim 11:501–522

Hong S-Y, Pan H-L (1996) Nonlocal boundary layer vertical diffusion in a medium-range forecast model. Mon Wea Rev 122:3–26

Jiang X, Yang S, Li Y, Kumar A, Liu X, Zuo Z, Jha B (2012) Seasonal-to-Interannual prediction of the Asian summer monsoon in the NCEP climate forecast system version 2. J Clim 26:3708–3727

Kain JS (2004) The Kain-Fritsch convective parameterization: an update. J Appl Meteor 43:170–181

Kain JS, Fritsch JM (1993) Convective parameterization for mesoscale models: the Kain-Fritsch scheme. The Representation of Cumulus convection in Numerical Models. Meteor. Monogr. No. 46, Am Meteor Soc pp 165–170

Kalnay E, Coauthors (1996) The NCEP/NCAR 40-Year reanalysis project. Bull Amer Meteor Soc 77:437–471

Kanamitsu M, Ebusuzaki W, Woollen J, Yang S-K, Hnilo J, Fiorino M, Potter GL (2002) NCEP-DOE AMIP-II reanalysis (R-2). Bull Am Meteorol Soc 83:1631–1643

Kang I-S et al (2002) Intercomparison of the climatological variations of Asian summer monsoon precipitation simulated by 10 GCMs. Clim Dyn. doi:10.1007/s00382-002-0245-9

Kim H-M, Webster PJ, Curry JA, Toma VE (2012) Asian summer monsoon prediction in ECMWF system 4 and NCEP CFSv2 retrospective seasonal forecasts. Clim Dyn. doi:10.1007/s00382-012-1470-5

Kirtman BP, Min D (2009) Multimodel ensemble ENSO prediction with CCSM and CFS. Monthly Weather Rev 137:2908–2930

Kirtman BP, Shukla J (2002) Interactive coupled ensemble: a new coupling strategy for CGCMs. Geophys Res Lett. doi:10.1029/2002GL014834

Koster RD et al (2004) Regions of strong coupling between soil moisture and precipitation. Science 305:1138–1140

Krishnakumar K, Rajagopalan B, Cane MA (1999) On the weakening relationship between Indian monsoon and ENSO. Science 284:2156–2159

Krishnamurthy V, Goswami BN (2000) Indian Monsoon–ENSO relationship on interdecadal timescale. J Clim 13:579–595

Krishnamurti TN, Ramanathan Y (1982) Sensitivity of the monsoon onset to differential heating. J Atmos Sci 39:1290–1306

Kucharski F, Bracco A, Yoo JH, Molteni F (2007) Low-frequency variability of the Indian Monsoon–ENSO relationship and the Tropical Atlantic: the "Weakening" of the 1980s and 1990s. J Clim 20:4255–4266

LaRow T (2013) The impact of SST bias correction on North Atlantic Hurricane Retrospective Forecasts. Mon Wea Rev 141:490–498

Li H, Misra V (2013) Global seasonal climate predictability in a two tiered forecast system. Part II: boreal winter and spring seasons. Clim Dyn. doi:10.1007/s00382-013-1813-x

Mason SJ, Graham NE (1999) Conditional probabilities, relative operating characteristics, and relative operating levels. Weather Forecast 14:713–725

Mason SJ, Graham NE (2002) Areas beneath the relative operating characteristics (ROC) and levels (RROL) curves: statistical significance and interpretations. Quart J R Meteoro Soc 128:2145–2166

Meehl GA, Arblaster JM (2002) Indian monsoon GCM sensitivity experiments testing tropospheric biennial oscillation transition conditions. J Clim 15:923–944

Misra V (2008) Coupled interactions of the monsoons. Geophys Res Lett 35:1–7

Misra V, Li H, Wu Z, DiNapoli S (2013) Global seasonal climate predictability in a two tiered forecast system. Part I: Boreal summer and fall seasons. Clim Dyn. doi:10.1007/s00382-013-1812-y

Mitchell TD, Jones PD (2005) An improved method of constructing a database of monthly climate observations and associated high resolution grids. Int J Climatol 25:693–712

Palmer TN (1994) Chaos and predictability in forecasting the monsoons. Proc Indian Natl Sci Acad 60A:57–66

Saha S, Moorthi S, Wu X, Wang J, Nadiga S, Tripp P, Pan H-L, Behringer D, Hou Y-T, Chuang H, Iredell M, Michael Ek, Meng J, Yang R, van den Dool H, Zhang Q, Wang W, Chen M (2012)

The NCEP Climate Forecast System Version 2. (Submitted to the Journal of Climate.) Available from http://cfs.ncep.noaa.gov/cfsv2.info/CFSv2_paper.pdf

Shukla J, Paolino DA (1983) The Southern Oscillation and longrange forecasting of the summer monsoon rainfall over India. Mon Wea Rev 111:1830–1837

Sikka DR (1980) Some aspects of the large-scale fluctuations of summer monsoon rainfall over India in relation to fluctuations in the planetary and regional scale circulation parameters. Proc Indian Natl Acad Sci 89:179–195

Slingo JM (1987) The development and verification of a cloud prediction model for the ECMWF model. Quart J R Meteor Soc 113:899–927

Sperber KR, Palmer TN (1996) Interannual tropical rainfall variability in general circulation model simulations associated with the Atmospheric Model Intercomparison Project. J Clim 9:2727–2750

Sperber KR et al (2001) Dynamical seasonal predictability of the Asian summer monsoon. Mon Wea Rev 129:2226–2248

Straus D, Shukla J (2002) Does ENSO force the PNA? J Clim 15:2340–2358

Tao S, Chen L (1987) A review of recent research on the East Asian summer monsoon. In: Chang C-P, Krishnamurti TN (eds) China, Monsoon meteorology. Oxford University Press, Oxford, pp 60–92

Tiedtke M (1983) The sensitivity of the time-mean large-scale flow to cumulus convection in the ECWMF model. In: Proceedings of ECMWF workshop on convection in large-scale models. European Centre for Medium-Range Forecasts, Reading, United Kingdom, pp 297–316

Trenberth KE, Hurrell JW, Stepanaik DP (2006) The Asian Monsoon: global perspectives. In: Wang B (ed) The Asian Monsoon. Springer/Praxis Publishing Co, New York, pp 67–87

Waliser DE et al (2002) AGCM simulations of intraseasonal variability associated with the Asian summer monsoon. Clim Dyn 21:423–446

Walker GT, Bliss EW (1932) World Weather V. Mem Roy Meteor Soc 4:53–84

Wang B, J-Y Lee et al (1980–2004) Advance and prospect of seasonal prediction: assessment of the APCC/CliPAS 14-model ensemble retroperspective seasonal prediction (1980–2004). Clim Dyn 33: 90. doi:10.1007/s00382-008-0460-0

Wang B, Fan Z (1999) Choice of South Asian Summer Monsoon Indices. Bull Am Meteor Sci 80:629–638

Wang B, Clemens S, Liu P (2003) Contrasting the Indian and East Asian monsoons: implications on geologic time scale. Mar Geol 201:5–21

Wang B, Kang IS, Lee JY (2004) Ensemble simulations of Asian-Australian Monsoon Variability by 11 AGCMs. J Clim 17:803–818

Wang B et al (2005a) Fundamental challenge in simulation and prediction of summer monsoon rainfall. Geophys Res Lett 32:L15711. doi:10.1029/2005GL022734

Wang B, Ding Q, Kang I-S et al (2005b) Fundamental challenges in simulation and prediction of summer monsoon rainfall. Geophys Res Lett 32(15):L15711

Wang B, Lee JY, Kang IS, Shukla J, Kug JS, Kumar A, Schemm J, Luo JJ, Yamagata T, Park CK (2008a) How accurately do coupled climate models predict the leading modes of Asian-Australian interannual variability? Clim Dyn 30:605–619

Wang B et al (2008b) Advance and prospectus of seasonal prediction: assessment of the APCC/CliPAS 14-model ensemble retrospective seasonal prediction (1980–2004). Clim Dyn. doi:10.1007/s00382-008-0460-0

Wang B, Ding Q, Joseph V (2009) Objective definition of the Indian Summer Monsoon onset using large scale winds. J Clim 22:3303–3316

Webster PJ (2006) The coupled monsoon system. In: Wang B (ed) The Asian Monsoon. Praxis, pp 1–66

Webster PJ, Magana VO, Palmer TN, Shukla J, Tomas RA, Yanai M, Yasunari T (1998) Monsoons: processes, predictability, and the prospects for prediction. J Geophys Res 103:14451–14510

Wu R, Kirtman BP (2005) Role of Indian and Pacific Ocean air-sea coupling in tropical atmospheric variability. Clim Dyn 25:155–170

Xie P, Arkin PA (1997) Global precipitation: a 17-year monthly analysis based on gauge observations, satellite estimates, and numerical model outputs. Bull Amer Meteorol Soc 78:2539–2558

Zhou T, Wu B, Wang B (2009) How well do atmospheric general circulation models capture the leading modes of the interannual variability of the Asian–Australian Monsoon? J Climate 22:1159–1173